Anomalous V p / V s Ratios at Seismic Frequencies Might Evidence Highly Damaged Rocks in Subduction Zones

Lucas Pimienta, Alexandre Schubnel, Marie Estelle Solange Violay, Jerome Fortin, Yves Gueguen, H Lyon-Caen

Geophysical Research Letters

RESEARCH LETTER
10.1029/2018GL080132

Anomalous V_p/V_s Ratios at Seismic Frequencies Might Evidence Highly Damaged Rocks in Subduction Zones

Lucas Pimienta[1,2], Alexandre Schubnel[2], Marie Violay[1], Jérôme Fortin[2], Yves Guéguen[2], and Hélène Lyon-Caen[2]

[1]Laboratory of Experimental Rock Mechanics, Ecole Polytechnique Federale de Lausanne, Lausanne, Switzerland, [2]Laboratoire de Géologie, Ecole Normale Supérieure, CNRS, PSL University, Paris, France

Key Points:
- First measurements of V_p/V_s in isotropic crustal rocks that quantitatively fit with the anomalously high values at subduction zones
- Anomalous V_p/V_s might evidence large degree of damage, opened by quasi-lithostatic fluid pressure, in isotropic rocks of any mineralogy
- Permeability ranges directly inferred from the reported V_p/V_s values could be very large

Supporting Information:
- Supporting Information S1
- Data Set S1

Correspondence to:
L. Pimienta,
lucas.pimienta@epfl.ch

Citation:
Pimienta, L., Schubnel, A., Violay, M., Fortin, J., Guéguen, Y., & Lyon-Caen, H. (2018). Anomalous V_p/V_s ratios at seismic frequencies might evidence highly damaged rocks in subduction zones. *Geophysical Research Letters*, *45*, 12,210–12,217. https://doi.org/10.1029/2018GL080132

Received 22 AUG 2018
Accepted 19 SEP 2018
Accepted article online 10 OCT 2018
Published online 20 NOV 2018

Abstract Unusually high compressional (*P*) to shear (*S*) wave velocity ratios (V_p/V_s) were measured at different subduction zones and interpreted as fluid-pressurized regions. Because no laboratory data reported such high values in isotropic rocks, mineralogical or anisotropic constrains were assumed. However, fluid-saturated rocks' V_p/V_s is a frequency-dependent property so that standard laboratory measurements cannot be directly upscaled to the field. Using a new methodology, we measured the property in the elastic regime relevant to field measurements for diverse lithologies. We obtained extreme V_p/V_s values, consistent with those reported at seismic frequency in the field. Consistently with a model, it shows that if high fluid pressure is a key factor, anomalous V_p/V_s values could evidence intense degrees of microfracturation in isotropic rocks, whichever its mineralogical content. The permeability of these regions could be larger than 10^{-16} m^2.

Plain Language Summary Anomalous seismic properties measured at subduction zones across the globe have been linked to the occurrence of earthquakes or tremors. However, different physical causes were postulated to interpret such seismic properties, and none of the laboratory measurements quantitatively fitted with those anomalous values. From laboratory measurements dedicated to link with field ones, we report the first data set that fits with field measurements observed at subduction zones. We show that such values might evidence a large degree of microfracturing, opened by high pore fluid pressure, in isotropic rocks of any mineralogy.

1. Introduction

Anomalously high compressional (*P*) to shear (*S*) wave velocity ratios, V_p/V_s, were reported (Figure 1a) at several subduction zones (Audet & Bürgmann, 2014; Audet & Kim, 2016) such as Cascadia (Audet et al., 2009), Central Mexico (Kim et al., 2010), Costa Rica (Audet & Schwartz, 2013), Alaska (Audet & Schwartz, 2013), and the Nankai trough (Kodaira, 2004; Shelly et al., 2006). Because V_p/V_s directly relates to the Poisson's ratio of solids via $(V_p/V_s)^2 = 2(1-\nu)/(1-2\nu)$, the Poisson's ratio of fluids being 0.5, high V_p/V_s ratios were generally attributed to the existence of high pore fluid pressures (Audet et al., 2009; Audet & Bürgmann, 2014; Audet & Schwartz, 2013; Peacock et al., 2011). Indeed, laboratory measurements qualitatively showed an increase in the rock Poisson's ratio as fluid pressure increased near lithostatic pore fluid pressure (Audet & Bürgmann, 2014; Christensen, 1984; Peacock et al., 2011). However, no laboratory results to date reported values large enough to fit with seismic observations in subduction zones (Christensen, 2004; Peacock et al., 2011). To further account for the discrepancy between laboratory measurements and field scale observations, additional hypotheses were formulated as (i) rocks of specific mineralogy (Audet & Bürgmann, 2014; Christensen, 2004; Peacock et al., 2011) with high Poisson's ratio (Abers & Hacker, 2016; Christensen, 1996), (ii) partial melting (Ji et al., 2009), or (iii) anisotropy (Christensen, 2004; Song & Kim, 2012; Wang et al., 2012). For instance, these high V_p/V_s regions were assumed to be depleted in quartz (Audet & Bürgmann, 2014) because quartz Poisson's ratio is small (Abers & Hacker, 2016; Arns et al., 2002; Christensen, 1996; Hacker & Abers, 2004).

An additional complexity is seldom accounted for when comparing field and laboratory measurements (Müller et al., 2010): While field measurements are performed at the subsonic frequency (i.e., about 1 Hz), standard laboratory measurements are performed at ultrasonic frequencies (i.e., 1 MHz). Recent experimental studies (Pimienta, Fortin, & Guéguen, 2016b) showed that Poisson's ratio (or V_p/V_s) of fluid-saturated rocks is a

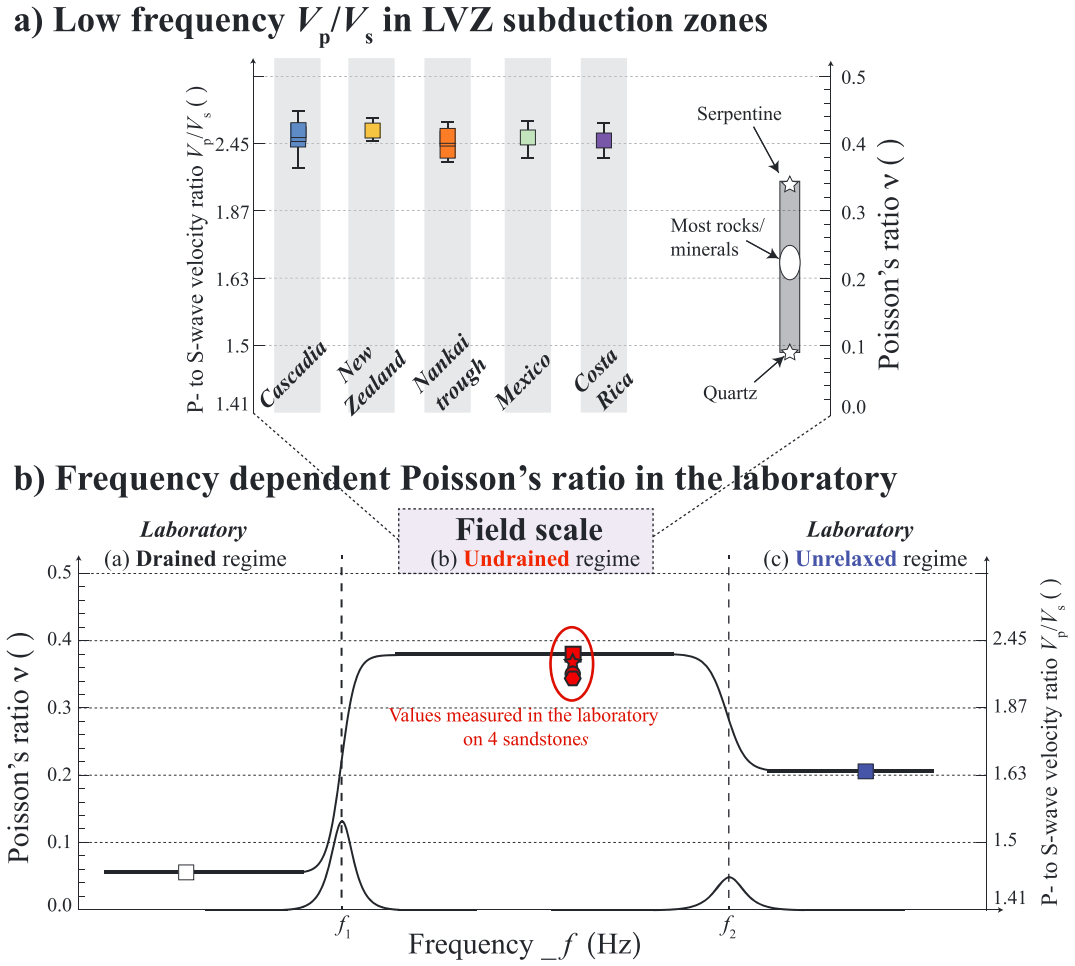

Figure 1. (a) V_P/V_S reported for the low velocity zones of different subduction zones across the globe (Audet & Bürgmann, 2014; Audet & Schwartz, 2013) as compared to minerals Poisson's ratio (Christensen, 1996); (b) schematic frequency dependence of Poisson's ratio (or V_P/V_S) based on recent results (Pimienta, Fortin, Borgomano, et al., 2016a), highlighting the comparison expected between laboratory and field measurements. The figure highlights measurements obtained for an isotropic Fontainebleau sandstone, in the three elastic regimes (squares), and reports for comparison values found (Pimienta et al., 2017) for three other isotropic sandstones in the undrained regime.

frequency-dependent property, exhibiting important variations over the measured frequency range (Figure 1b and Figure A1 in the supporting information). Frequency-dependent variations of the Poisson's ratio in fluid saturated rocks generally originate from two different viscous fluid-flow dissipation mechanisms, separating three distinct elastic regimes (Adelinet et al., 2010): the drained, undrained, and unrelaxed/isolated regimes.

In the laboratory, standard ultrasonic methods either measure the drained (Figure 1b, left) or unrelaxed elastic response (Figure 1b, right) when samples are respectively dry or fluid-saturated. At the field scale, because the characteristic frequencies are expected to be far apart (Figure A1), the relevant elastic regime is often the undrained one (Figure 1b, center). For instance, low Poisson's ratio is measured both in the drained (Figure 1b, left) and in the unrelaxed (Figure 1b, right) regimes in a sandstone sample (Pimienta, Fortin, & Guéguen, 2016b). In the undrained regime (Figure 1b, center), for the same rock, anomalously high Poisson's ratios are measured, as consistently observed in three additional sandstones (Pimienta et al., 2017). Interestingly, Poisson's ratios of 0.35–0.38 corresponded to V_P/V_S ranging between 2 and 2.4, that is, close to the largest values reported (Audet et al., 2009; Audet & Bürgmann, 2014) at the field scale.

Table 1
Porosity, Ultrasonic P and S Wave Velocities of the Dry Rock Samples at Room Conditions

	Porosity	*P* wave velocity	*S* wave velocity
Carrara marble	0.3%	6.2 km/s	3.3 km/s
Westerly granite (*WGs*)	0.7%	5.5 km/s	3.1 km/s
Azores andesite (*Pan*)	5.8%	2.0 km/s	1.2 km/s
Icelandic basalt (*IBas*)	2.6%	4.7 km/s	2.6 km/s
Fontainebleau sandstone (*Fo3*)	3.2%	5.3 km/s	3.4 km/s
Fontainebleau sandstone (*Fo7*)	7.3%	3.1 km/s	2.0 km/s
WGs @ 500 °C	1.8%	2.4 km/s	1.6 km/s
Fo3 @ 500 °C	4.1%	3.5 km/s	2.3 km/s

From these observations, this work aims at investigating the undrained V_p/V_s of most crustal rocks and explaining it physically with a simple model. Then, using the V_p/V_s values reported from the field scale, ranges in permeability will be provided.

2. Method

2.1. Rock Samples

For the purpose of the study, the rock samples chosen (Table 1) are of (i) Carrara Mable (i.e., *CarMbl*), a crystalline rock of pure content (i.e., 100%) in randomly oriented calcite minerals (Delle Piane et al., 2015; Schubnel et al., 2006); (ii) Westerly granite (i.e., *WGs*), a well-known isotropic and homogeneous rock (Faulkner et al., 2006; Wang et al., 2012); (iii) an Andesite sample from Azores Islands, Portugal (i.e., *PAn*); (iv) an Icelandic Basalt (i.e., *IBas*), homogeneous and isotropic at the sample scale (Adelinet, 2010; Adelinet et al., 2010); and (v) two samples of clean (i.e., 100% quartz) Fontainebleau sandstone, of 3% (i.e., *Fo3*) and 7% (i.e., *Fo7*) porosity. The sandstone is composed of randomly oriented quartz grains cemented by quartz, usually homogeneous and isotropic at the sample scale (Pimienta et al., 2014), and very similar to a quartzite once the content of spherical pores tends to zero (i.e., low porosity samples). Hence, the two samples can consistently be assumed to exhibit physical properties very similar to what one may expect for quartzite.

For the two samples of *WGs* and *Fo3*, after measurement of Poisson's ratio on the intact sample, the two samples were then put in the oven for thermal treatment at 500 °C—with small temperature ramps (i.e., about 5 °C/min variation)—and then measured gain with the same procedure. The thermal treatment method was shown to induce a large and isotropic degree of microfracturing due to the mismatch in thermal expansion of the grains in initially isotropic rocks (Fredrich & Wong, 1986; Nasseri et al., 2007, 2009).

All rock samples have an overall porosity below 7%. In case of the initial samples, all except for *Fo7* and *PAn* show high *P* and *S* wave velocity. Comparing those data with existing theories (Guéguen & Kachanov, 2011; Walsh, 1966), a low content in initial microcrack density is inferred for most samples except those two. Applying thermal treatment on *WGs* and *Fo3*, the rock samples' porosity increases and *P* and *S* wave velocities decrease, which is consistent with the creation of microcracks (Nasseri et al., 2009; Wang et al., 2013).

2.2. Measuring Procedure

Rock samples, equipped with pairs of axial and radial strain gages, are jacketed and enclosed between end-platens so that oil confining pressure and pore fluid pressure can be applied independently to the rock sample. The sample is consecutively measured under dry and fully saturated conditions at different values of confining and pore pressures. The piston is equipped with a piezo-electric actuator that allows applying axial stress oscillations of low amplitude over a wide frequency band (Borgomano et al., 2017; Pimienta et al., 2015b). At a given static pressure, axial stress oscillations of strain amplitudes below 10^{-5} are applied to the rock sample at different frequencies (Figure 2). This calibrated method allows reaching precisely Poisson's ratio of rock samples under purely isotropic stress conditions (Pimienta et al., 2015b; Pimienta, Fortin, & Guéguen, 2016b).

An example of measurements for different frequencies of oscillating stresses is reported for the microcracked *Fo3* sample (Figure 2). As observed from the raw data (Figure 2a), when normalizing the data with respect to the axial strain oscillations, radial strain oscillations largely depend on both the fluid and the frequency, with maximum amplitudes in the frequency range of 1–10 Hz. Inferring Poisson's ratio (Figure 2b) indeed shows a frequency-dependent increase up to 1–10 Hz and then decrease beyond this frequency. The variation is very similar to that observed (Pimienta, Fortin, & Guéguen, 2016b) and schematically highlighted for *Fo7* (Figure A1a).

In this work, only the measured values of Poisson's ratio under dry and fluid-saturated conditions in the undrained regime—relevant to the field's scale—are of interest. Following an assessed procedure (Pimienta et al., 2015a, 2015b), the undrained regime corresponds to the frequency beyond which fluid cannot flow anymore out of the sample and that remains low enough not to be in the unrelaxed regime (Figure A1). As shown from earlier experimental work (Pimienta, Fortin, & Guéguen, 2016b), this distinction

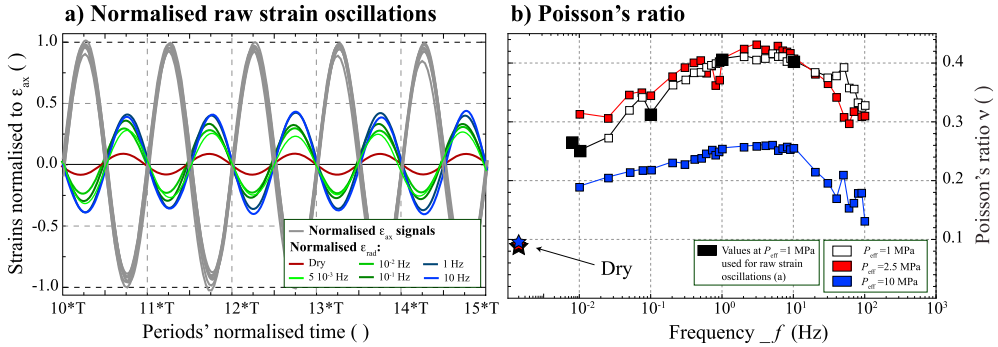

Figure 2. Principle, for the microcracked *Fo3*, of the acquired (a) strain oscillations for different frequencies at a Terzaghi effective pressure of 1 MPa, normalized as a function of the axial strain (gray curves) and time period *T*, and (b) inferred Poisson's ratio, obtained from the linear regressions between the radial and the axial strain, as a function of the frequency of the oscillations. The colors in (a) are from red in the dry/drained regime to black-blue in the undrained regime, with varying degrees of green in the transition from drained to undrained. The black squares in (b) are the values that correspond to the plotted oscillations in (a).

also corresponds to a maximum value in the rock Poisson's ratio (Figure 2b). To account for the dependence of Poisson's ratio to confining and pore pressure, the samples are measured as a function of frequency at varying Terzaghi effective pressures ($P_{eff} = P_c - p_f$) in the range of [1–30] MPa (Figure 2). The peaked Poisson's ratio under dry/drained and undrained regime, measured as a function of P_{eff} (Figure A2), is then inferred as a function of p_f. Where $P_{eff} = P_c - p_f$ equally links the decrease P_c or increase in p_f to the decrease in P_{eff} (i.e., Arrow in Figure A2e).

2.3. Model for Cracked Rocks

A simple modeling approach is used (Adelinet et al., 2011) by combining effective medium theories (Guéguen & Kachanov, 2011; Kachanov et al., 1994) and poroelasticity (Biot, 1956; Gassmann, 1951). The

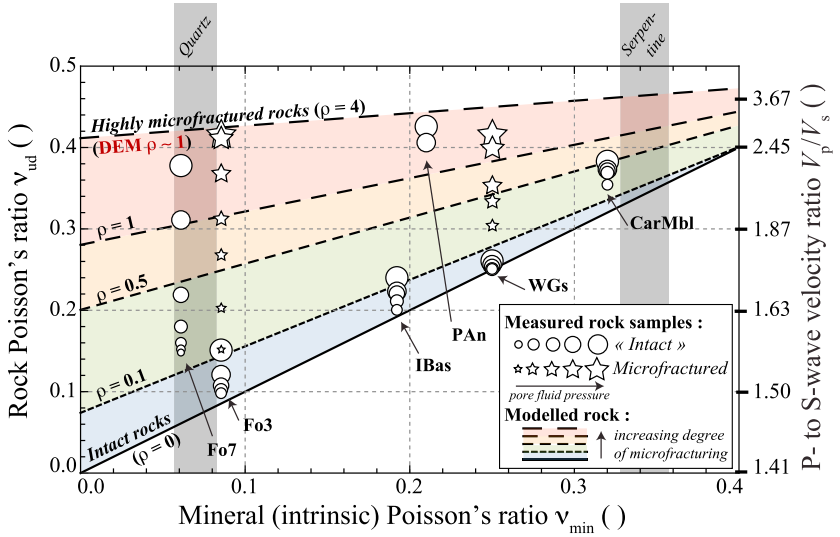

Figure 3. Comparison between measurements and model predictions of Poisson's ratio in the undrained regime (i.e., field's V_p/V_s) over the whole range of existing mineral intrinsic Poisson's ratio. For the predictions, the undrained ν_{ud} of a mineral-pure microcracked, isotropic, water-saturated rock is predicted as a function of the mineral ν_{min} for different values of microcrack density ρ (lines with different dashing spaces). The modeling methods (e.g., differential effective medium theory) are detailed in Figure A3. For the measurements, the *x* axis is obtained from measured ν_d of the dry rock, and the *y* axis is the ν_{ud} measured on the water-saturated rock. The increasing symbol size highlights the increase in pore fluid pressure, hence decrease in Terzaghi effective pressure (Figure A2) in the range of [1;15] MPa. Samples measured are of (i) marble (*CarMbl*), (ii) granite (*WGs*), (iii) andesite (*PAn*), (iv) basalt (*IBas*), and (v) quartz-pure sandstone, of 3% (*Fo3*) and 7% (*Fo7*) porosity. All rock samples are measured in their natural state (hence "intact"), and two measurements are made in *Fo3* and *WGs* samples after thermal treatment to 500 °C (hence "microfractured").

model assumes a pure homogeneous and isotropic mineral phase in which porous inclusions are introduced. In porous rocks such as sandstones or basalts, two types of inclusions are often considered (Adelinet et al., 2011; Fortin et al., 2014): (i) spherical inclusions, for the pressure-independent porosity, and (ii) thin elongated spheroidal inclusions (i.e., degree of microcracking), which is the intrinsic cause for the pressure dependence of rocks properties (Walsh, 1965a, 1965b, 1965c). From changing the compressibility of the fluid, this inclusion model allows predicting the effective properties of the medium in dry/drained (υ_d) and water-saturated unrelaxed (υ_{ur}) regimes. The undrained regime (υ_{ud}) is then deduced by combining the Biot-Gassmann equations (Gassmann, 1951) with that of the drained (i.e., dry) medium (Adelinet et al., 2011).

With the aim to test the measurements, predictions are made for different mineral-constituting matrices to span the whole range of accessible Poisson's ratio values, that is, from quartz (ν_{min} = 0.07) to plagioclase (ν_{min} = 0.35). As reported in the literature (Arns et al., 2002; Christensen, 1996), the whole range of dry rocks found in nature fall within these bounds (Figure 1a). Under undrained conditions, the bulk modulus of water (i.e., K_{wat} = 2.2 GPa) is used for comparison with direct measurements.

3. Results

Values of ν_{ud}—measured for different P_{eff} (Figure A2)—are reported as a function of the measured Poisson's ratio ν_d of the dry samples (Figure 3) spanning a wide range, from quartz (ν_{min} = 0.06) up to calcite (ν_{min} = 0.32). Basalt (*IBas*), andesite (*PAn*), and granite (*WGs*) samples have intermediate ν_d ranging between 0.2 and 0.25. In the undrained regime, small variations are observed for ν_{ud} of *CarMbl*, *WGs*, *IBas*, and *Fo3*, the larger values corresponding to the highest pore fluid pressure (i.e., P_{eff} = 1 MPa) tested. In comparison, Fontainebleau sandstone sample *Fo7* and the andesite *Pan* both exhibited large variations, from low ν_d to ν_{ud} values reaching 0.38–0.42 at highest p_f (i.e., P_{eff} = 1 MPa). Although with quite different initial ν_d values, the similar ν_{ud} values for these two samples (i.e., *Fo7* and *PAn*) arises from an initially large degree of microfracturation or open grain contacts (Pimienta, Fortin, & Guéguen, 2016b). This is further confirmed by measures performed on thermally damaged samples *Fo3* and *WGs*, for which ν_{ud} increased in dramatic ways after microcracking to 500 °C, while little variations were observed on the "intact" rock sample. For these two samples, the undrained Poisson's ratio ν_{ud} reached values as high as 0.42 (i.e., V_p/V_s of 2.69) when pore fluid pressure was maximum (i.e., P_{eff} = 1 MPa), which fits with the dramatic values of V_p/V_s = 2.69 measured at the field scale. Once pore fluid pressure was decreased (i.e., P_{eff} = 15 MPa), ν_{ud} decreased down to 0.15 for *Fo3* because of microcrack closure (Walsh, 1965c).

Measurements are compared to the model, coupling poroelasticity and effective medium theories (Adelinet et al., 2011), which predicts the effective undrained Poisson's ratio of homogeneous, isotropic, and microcracked water-saturated rocks (Figure 3). Predictions are made for increasing degrees of microfracturing. As the crack density increases, the model predicts an increase in ν_{ud}. Its sensitivity to the presence of microcracks is larger when the intact mineral Poisson's ratio (hence ν_d) is low. In other words, microcracks have larger effects on ν_{ud} of quartz-rich rocks than for calcite-rich or mafic ones. The model also predicts quasi-mineral-independent values near 0.5 at the onset of fragmentation, when materials are too heavily damaged to maintain their solid structure.

The model assumes opened microcracks, which intrinsically implies that the effective pressure is low. Hence, both the model predictions and the laboratory measurements demonstrate that, independently of mineralogical constrains, low effective pressure (via quasi-lithostatic pore fluid pressure) in a highly microfractured medium can lead to anomalously high Poisson's ratio values of 0.4 and above (i.e., V_p/V_s = 2.69). The model also demonstrates that Poisson's ratio dispersion is mainly observed in the presence of compliant porosity, that is, crack-like rather than equant pores. Additional laboratory measurements (Pimienta, Fortin, & Guéguen, 2016b) on a 8% porosity, almost crack-free, Fontainebleau sandstone confirm that Poisson's ratio remains low (i.e., 0.15) when the pore fluid pressure was very high (i.e., P_{eff} = 1 MPa).

4. Discussion

Three main candidates had been postulated to explain anomalous V_p/V_s: (1) anisotropy, (2) mafic composition, or possibly (3) plasticity. From laboratory measurements and modeling, accounting for the elastic

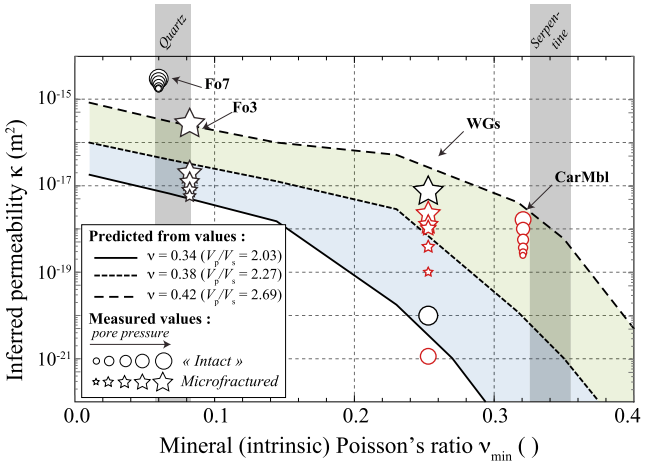

Figure 4. Range in permeability predicted from a range of high V_p/V_s values reported from field's scale measurements as a function of the rock mineral Poisson's ratio. The colored areas (i.e., green then blue) highlight the evolution in permeability from an extremely high V_p/V_s (dashed line) to a high one (plain line). Permeability was either (i) measured (black symbols) as a function of P_{eff} (hence increasing p_f) on the microcracked *Fo3* sample, the "intact" *Fo7*, and the microcracked *WGs* at lowest P_{eff} = 1 MPa or (ii) attained (red symbols) from published works (Delle Piane et al., 2015; Loaiza et al., 2012; Nasseri et al., 2009). It is again represented (i.e., symbols of varying sizes) as a function of the dry rock Poisson's ratio for different Terzaghi effective pressures, that is, pore fluid pressure.

regime relevant to the field measurements, we show that anomalous V_p/V_s do not necessarily imply anisotropy or mafic composition. Such high values can be observed even in isotropic quartz-pure rocks, at ambient temperature. The sole condition for those rocks is its large degree of microfracturation opened by a quasi-lithostatic fluid pressure.

The rocks were measured at ambient temperature and low confining pressure conditions, and the model intrinsically assumes for the rock to be elastic. At the depth of those zones, however, pressure and temperature are high. If Terzaghi effective pressure applies, the relevant quantity is $P_{eff} = P_c - p_f$ so that the earlier results hold (Figure 3). Depending on rock types (e.g., mineralogy), at high temperatures, viscoplasticity could, however, occur (Ji et al., 2009). Pore fluid (i.e., water) properties, such as viscosity, density, and compressibility, also depend on the *P-T* conditions. While fluid viscosity controls the characteristic cutoff frequencies separating the elastic regimes (Figure A1), fluid compressibility is in turn expected to affect the magnitude of υ_{ud} values, for example, from gas to water. Within the ranges of 0–2 GPa and 0–1,000 °C, (i) model predictions of υ_{ud} only depend loosely on the water compressibility (Figure A4) so that the results will remain within an accuracy of 5% of that reported in Figure 3), and (ii) viscosity variations are well below that needed to affect the frequency dependences (Figure A1). In other words, the results hold whichever the *P-T* conditions of the fluid, including the ones relevant of subduction zones.

Permeability variations near and in these zones may promote the observed episodic tremors and slip (Audet et al., 2009; Audet & Bürgmann, 2014; Audet & Kim, 2016; Peacock et al., 2011; Yamashita & Schubnel, 2016). Using a micromechanical model, following earlier interpretations (i.e., Figure 3), we can assess the magnitudes of permeability expected from the high V_p/V_s measured. A percolation model of permeability (Benson et al., 2006; Gueguen & Dienes, 1989) predicts that in a microcracked medium, the permeability is $\kappa_c = \frac{2}{15} f_c w^2 \xi \rho$, where w is the crack aperture and ρ and ξ are the crack density and aspect ratio (i.e., ratio of aperture over diameter). f_c is the percolation factor, which describes the connectivity of the crack network (Gueguen & Dienes, 1989), that is, approximated as $f_c = \frac{9}{4}\left(\frac{\pi^2}{4}\rho - \frac{1}{3}\right)^2$.

From the elastic model, Poisson's ratios of 0.34, 0.38, or 0.42 (i.e., V_p/V_s of 2.03, 2.27, or 2.69) are uniquely related to values of crack density ρ and intrinsic Poisson's ratio (Figure 3). Permeability could thus be directly inferred, as qualitatively attempted here (Figure 4) by assuming realistic values of w = 0.7 μm and $\xi = 5\ 10^{-3}$ (Benson et al., 2006). Predicted values are reported as a function of the mineral Poisson's ratio (Figure 4). Measurements of the various lithologies investigated as a function of P_{eff} fall within the predicted range. For values of V_p/V_s = 2.69, depending on the lithology, a minimum permeability that ranges between 10^{-19} and 10^{-15} m^2 is predicted. Because w and ξ vary between rocks, and as a function of P_{eff}, Figure 4 does not aim at being quantitative but rather at highlighting that very high permeability could be observed. Again, rock plasticity or anisotropy could affect the permeability tensor inferred. The common origin of local high pore fluid pressure, important microcracking, and large increase in permeability might arise from dehydrating rocks, as suggested by recent laboratory work (Brantut et al., 2012).

5. Conclusion

Accounting for the frequency dependence of seismic properties, and in particular for V_p/V_s, we show that the unusually high values observed at subduction zones can be attained in the laboratory. In the relevant frequency range, we measured extreme values of V_p/V_s in crustal rocks of very different mineralogical composition, hence very different matrix Poisson's ratio. The necessary conditions are a near-lithostatic fluid pressure and a large degree of microfracturation of the rocks. All the conclusions are supported by a micromechanical model, which further suggests that a crack porosity is required for such effects. Combining the

models for elasticity and permeability, large permeability could be inferred from the V_p/V_s measured in subduction zones.

Acknowledgments
The authors wish to thank G. Abers and an anonymous reviewer for their constructive comments. The data sets used in this work are reported as supplementary tables (SI file). Further questions can be directly asked to the corresponding author. The authors thank Y. Pinquier for technical support. This work was allowed by the partial support for the EPFL and Marie Curie Fellowship of LP, by the MSCA (PROGRESS, project 665667) and the Swiss Competence Center for Energy Research (SCCER).

References

Abers, G. A., & Hacker, B. R. (2016). AMATLAB toolbox and Excel workbook for calculating the densities, seismic wave speeds, and major element composition of minerals and rocks at pressure and temperature. *Geochemistry, Geophysics, Geosystems*, *16*, 4494–4506. https://doi.org/10.1002/2015GC006070

Adelinet, M. (2010). Du terrain au laboratoire, Étude des propriétés élastiques du basalte Sciences de la Terre. Université du Maine, Français.

Adelinet, M., Fortin, J., & Guéguen, Y. (2011). Dispersion of elastic moduli in a porous-cracked rock: Theoretical predictions for squirt-flow. *Tectonophysics*, *503*(1–2), 173–181. https://doi.org/10.1016/j.tecto.2010.10.012

Adelinet, M., Fortin, J., Guéguen, Y., Schubnel, A., & Geoffroy, L. (2010). Frequency and fluid effects on elastic properties of basalt: Experimental investigations. *Geophysical Research Letters*, *37*, L02303. https://doi.org/10.1029/2009GL041660

Arns, C. H., Knackstedt, M. A., & Pinczewski, W. V. (2002). Accurate Vp:Vs relationship for dry consolidated sandstones. *Geophysical Research Letters*, *29*(8), 1202. https://doi.org/10.1029/2001GL013788

Audet, P., Bostock, M. G., Christensen, N. I., & Peacock, S. M. (2009). Seismic evidence for overpressured subducted oceanic crust and megathrust fault sealing. *Nature*, *457*(7225), 76–78. https://doi.org/10.1038/nature07650

Audet, P., & Bürgmann, R. (2014). Possible control of subduction zone slow-earthquake periodicity by silica enrichment. *Nature*, *510*(7505), 389–392. https://doi.org/10.1038/nature13391

Audet, P., & Kim, Y. H. (2016). Teleseismic constraints on the geological environment of deep episodic slow earthquakes in subduction zone forearcs: A review. *Tectonophysics*, *670*, 1–15. https://doi.org/10.1016/j.tecto.2016.01.005

Audet, P., & Schwartz, S. Y. (2013). Hydrologic control of forearc strength and seismicity in the Costa Rican subduction zone. *Nature Geoscience*, *6*(10), 852–855. https://doi.org/10.1038/ngeo1927

Benson, P. M., Schubnel, A., Vinciguerra, S., Trovato, C., Meredith, P., & Young, R. P. (2006). Modeling the permeability evolution of micro-cracked rocks from elastic wave velocity inversion at elevated isostatic pressure. *Journal of Geophysical Research*, *111*, B04202. https://doi.org/10.1029/2005JB003710

Biot, M. A. (1956). Theory of propagation of elastic waves in a fluid-saturated porous solid. I. Low-frequency range. *The Journal of the Acoustical Society of America*, *28*(2), 168–178. https://doi.org/10.1121/1.1908239

Borgomano, J. V. M., Pimienta, L., Fortin, J., & Guéguen, Y. (2017). Dispersion and attenuation measurements of the elastic moduli of a bimodal-porosity limestone. *Journal of Geophysical Research: Solid Earth*, *122*, 2690–2711. https://doi.org/10.1002/2016JB013816

Brantut, N., Schubnel, A., David, E. C., Héripré, E., Guéguen, Y., & Dimanov, A. (2012). Dehydration-induced damage and deformation in gypsum and implications for subduction zone processes. *Journal of Geophysical Research*, *117*, B03205. https://doi.org/10.1029/2011JB008730

Christensen, N. I. (1984). Pore pressure and oceanic crustal seismic structure. *Geophysical Journal of the Royal Astronomical Society*, *79*(2), 411–423. https://doi.org/10.1111/j.1365-246X.1984.tb02232.x

Christensen, N. I. (1996). Poisson's ratio and crustal seismology. *Journal of Geophysical Research*, *101*(B2), 3139–3156. https://doi.org/10.1029/95JB03446

Christensen, N. I. (2004). Serpentinites, peridotites, and seismology. *International Geology Review*, *46*(9), 795–816. https://doi.org/10.2747/0020-6814.46.9.795

Delle Piane, C., Arena, A., Sarout, J., Esteban, L., & Cazes, E. (2015). Micro-crack enhanced permeability in tight rocks: An experimental and microstructural study. *Tectonophysics*, *665*, 149–156. https://doi.org/10.1016/j.tecto.2015.10.001

Faulkner, D. R., Mitchell, T. M., Healy, D., & Heap, M. J. (2006). Slip on "weak" faults by the rotation of regional stress in the fracture damage zone. *Nature*, *444*(7121), 922–925. https://doi.org/10.1038/nature05353

Fortin, J., Pimienta, L., Guéguen, Y., Schubnel, A., David, E. C., & Adelinet, M. (2014). Experimental results on the combined effects of frequency and pressure on the dispersion of elastic waves in porous rocks. *The Leading Edge*, *33*(6), 648–654. https://doi.org/10.1190/tle33060648.1

Fredrich, J. T., & Wong, T. (1986). Micromechanics of thermally induced cracking in three crustal rocks. *Journal of Geophysical Research*, *91*(B12), 743–764. https://doi.org/10.1029/JB091iB12p12743

Gassmann, F. (1951). Elasticity of porous media. *Vierteljahrsschrder Naturforschenden Gesselschaft*, *96*, 1–23.

Gueguen, Y., & Dienes, J. K. (1989). Transport properties of rocks from statistics and percolation 1. *Mathematical Geology*, *21*(1), 1–13. https://doi.org/10.1007/BF00897237

Guéguen, Y., & Kachanov, M. (2011). Effective elastic properties of cracked rocks an overview. Mechanics of Crustal Rocks. In *Mechanics of crustal rocks*, (pp. 73–125). Vienna: Springer.

Hacker, B. R., & Abers, G. A. (2004). Subduction factory 3: An Excel worksheet and macro for calculating the densities, seismic wave speeds, and H2O contents of minerals and rocks at pressure and temperature. *Geochemistry, Geophysics, Geosystems*, *5*, Q01005. https://doi.org/10.1029/2003GC000614

Ji, S., Wang, Q., & Salisbury, M. H. (2009). Composition and tectonic evolution of the Chinese continental crust constrained by Poisson's ratio. *Tectonophysics*, *463*(1–4), 15–30. https://doi.org/10.1016/j.tecto.2008.09.007

Kachanov, M., Tsukrov, I., & Shafiro, B. (1994). Effective moduli of solids with cavities of various shapes. *Applied Mechanics Reviews*, *47*(1S), S151. https://doi.org/10.1115/1.3122810

Kim, Y., Clayton, R. W., & Jackson, J. M. (2010). Geometry and seismic properties of the subducting Cocos plate in central Mexico. *Journal of Geophysical Research*, *115*, B06310. https://doi.org/10.1029/2009JB006942

Kodaira, S. (2004). High pore fluid pressure may cause silent slip in the Nankai trough. *Science*, *304*(5675), 1295–1298. https://doi.org/10.1126/science.1096535

Loaiza, S., Fortin, J., Schubnel, A., Gueguen, Y., Vinciguerra, S., & Moreira, M. (2012). Mechanical behavior and localized failure modes in a porous basalt from the Azores. *Geophysical Research Letters*, *39*, L19304. https://doi.org/10.1029/2012GL053218

Müller, T. M., Gurevich, B., & Lebedev, M. (2010). Seismic wave attenuation and dispersion resulting from wave-induced flow in porous rocks—A review. *Geophysics*, *75*(5), 75A147–75A164. https://doi.org/10.1190/1.3463417

Nasseri, M. H. B., Schubnel, A., Benson, P. M., & Young, R. P. (2009). Common evolution of mechanical and transport properties in thermally cracked westerly granite at elevated hydrostatic pressure. *Pure and Applied Geophysics*, *166*(5–7), 927–948. https://doi.org/10.1007/s00024-009-0485-2

Nasseri, M. H. B., Schubnel, A., & Young, R. P. (2007). Coupled evolutions of fracture toughness and elastic wave velocities at high crack density in thermally treated westerly granite. *International Journal of Rock Mechanics and Mining Sciences*, *44*(4), 601–616. https://doi.org/10.1016/j.ijrmms.2006.09.008

Peacock, S. M., Christensen, N. I., Bostock, M. G., & Audet, P. (2011). High pore pressures and porosity at 35 km depth in the Cascadia subduction zone. *Geology*, *39*(5), 471–474. https://doi.org/10.1130/G31649.1

Pimienta, L., Borgomano, J. V. M., Fortin, J., & Guéguen, Y. (2017). Elastic dispersion and attenuation in fully saturated sandstones: Role of mineral content, porosity, and pressures. *Journal of Geophysical Research: Solid Earth*, *122*, 9950–9965. https://doi.org/10.1002/2017JB014645

Pimienta, L., Fortin, J., Borgomano, J. V. M., & Guéguen, Y. (2016a). Dispersions and attenuations in a fully saturated sandstone: Experimental evidence for fluid flows at different scales. *The Leading Edge*, *35*(6), 495–501. https://doi.org/10.1190/tle35060495.1

Pimienta, L., Fortin, J., & Gueguen, Y. (2014). Investigation of elastic weakening in limestone and sandstone samples from moisture adsorption. *Geophysical Journal International*, *199*(1), 335–347. https://doi.org/10.1093/gji/ggu257

Pimienta, L., Fortin, J., & Guéguen, Y. (2015a). Bulk modulus dispersion and attenuation in sandstones. *Geophysics*, *80*(2), D111–D127. https://doi.org/10.1190/geo2014-0335.1

Pimienta, L., Fortin, J., & Guéguen, Y. (2015b). Experimental study of Young's modulus dispersion and attenuation in fully saturated sandstones. *Geophysics*, *80*(5), L57–L72. https://doi.org/10.1190/geo2014-0532.1

Pimienta, L., Fortin, J., & Guéguen, Y. (2016b). Effect of fluids and frequencies on Poisson's ratio of sandstone samples. *Geophysics*, *81*(2), D183–D195. https://doi.org/10.1190/geo2015-0310.1

Schubnel, A., Walker, E., Thompson, B. D., Fortin, J., Guéguen, Y., & Young, R. P. (2006). Transient creep, aseismic damage and slow failure in Carrara marble deformed across the brittle-ductile transition. *Geophysical Research Letters*, *33*, L17301. https://doi.org/10.1029/2006GL026619

Shelly, D. R., Beroza, G. C., Zhang, H., Thurber, C. H., & Ide, S. (2006). High-resolution subduction zone seismicity and velocity structure beneath Ibaraki Prefecture, Japan. *Journal of Geophysical Research*, *111*, B06311. https://doi.org/10.1029/2005JB004081

Song, T. R. A., & Kim, Y. (2012). Localized seismic anisotropy associated with long-term slow-slip events beneath southern Mexico. *Geophysical Research Letters*, *39*, L09308. https://doi.org/10.1029/2012GL051324

Walsh, J. B. (1965a). The effect of cracks in rocks on Poisson's ratio. *Journal of Geophysical Research*, *70*(20), 5249–5257. https://doi.org/10.1029/JZ070i020p05249

Walsh, J. B. (1965b). The effect of cracks on the compressibility of rock. *Journal of Geophysical Research*, *70*(2), 381–389. https://doi.org/10.1029/JZ070i002p00381

Walsh, J. B. (1965c). The effect of cracks on the uniaxial elastic compression of rocks. *Journal of Geophysical Research*, *70*(2), 399–411. https://doi.org/10.1029/JZ070i002p00399

Walsh, J. B. (1966). Seismic wave attenuation in rock due to friction. *Journal of Geophysical Research*, *71*(10), 2591–2599. https://doi.org/10.1029/JZ071i010p02591

Wang, X. Q., Schubnel, A., Fortin, J., David, E. C., Gueguen, Y., & Ge, H.-K. (2012). High Vp/Vs ratio: Saturated cracks or anisotropy effects? *Geophysical Research Letters*, *39*, L11307. https://doi.org/10.1029/2012GL051742

Wang, X. Q., Schubnel, A., Fortin, J., Guéguen, Y., & Ge, H. K. (2013). Physical properties and brittle strength of thermally cracked granite under confinement. *Journal of Geophysical Research: Solid Earth*, *118*, 6099–6112. https://doi.org/10.1002/2013JB010340

Yamashita, T., & Schubnel, A. (2016). Slow slip generated by dehydration reaction coupled with slip-induced dilatancy and thermal pressurization. *Journal of Seismology*, *20*(4), 1217–1234. https://doi.org/10.1007/s10950-016-9585-5